Calcif Tissue Int (2010) 86:397–403
DOI 10.1007/s00223-010-9353-4

Application of Structural Rigidity Analysis to Assess Fidelity of Healed Fractures in Rat Femurs with Critical Defects

Ara Nazarian · Lina Pezzella · Alan Tseng · Stephen Baldassarri · David Zurakowski · Christopher H. Evans · Brian D. Snyder

Received: 27 October 2009 / Accepted: 18 February 2010 / Published online: 31 March 2010

Abstract Approximately 6 million fractures occur each year in the United States, with an estimated medical and loss of productivity cost of $99 billion. As our population ages, it can only be expected that these numbers will continue to rise. While there have been recent advances in available treatments for fractures, assessment of the healing process remains a subjective process. This study aims to demonstrate the use of micro-computed tomography (μCT)-based structural rigidity analysis to accurately and quantitatively assess the progression of fracture healing over time in a rat model. The femora of rats with simulated lytic defects were injected with human BMP-2 cDNA at various time points postinjury (t = 0, 1, 5, 10 days) to accelerate fracture healing, harvested 56 days from time of injury, and subjected to μCT imaging to obtain cross-sectional data that were used to compute torsional rigidity. The specimens then underwent torsional testing to failure using a previously described pure torsional testing system. Strong correlations were found between measured torsional rigidity and computed torsional rigidity as calculated from both average ($R^2 = 0.63$) and minimum ($R^2 = 0.81$) structural rigidity data. While both methods were well correlated across the entire data range, minimum torsional rigidity was a better descriptor of bone strength, as seen by a higher Pearson coefficient and smaller *y*-intercept. These findings suggest considerable promise in the use of structural rigidity analysis of μCT data to accurately and quantitatively measure fracture-healing progression.

Keywords Fracture healing · Healing strength · Structural rigidity analysis · Segmental defect · Rat model

The authors have stated that they have no conflict of interest.

A. Nazarian (✉) · A. Tseng · S. Baldassarri · C. H. Evans · B. D. Snyder
Center for Advanced Orthopedic Studies, Beth Israel Deaconess Medical Center, Harvard Medical School, 330 Brookline Avenue, RN115, Boston, MA 02215, USA
e-mail: anazaria@bidmc.harvard.edu

D. Zurakowski
Department of Anesthesiology, Boston Children's Hospital, Harvard Medical School, Boston, MA, USA

B. D. Snyder
Department of Orthopedic Surgery, Boston Children's Hospital, Harvard Medical School, Boston, MA, USA

D. Zurakowski
Department of Surgery, Boston Children's Hospital, Harvard Medical School, Boston, MA, USA

L. Pezzella
Harvard Medical School, Boston, MA, USA

Approximately 6 million fractures occur each year in the United States, resulting in the largest (24%) total lifetime cost associated with any one type of injury [1]. Recent Centers for Disease Control (CDC) data estimate the medical and productivity cost of fractures at over $99 billion [2]. It is further estimated that 16% of Caucasian women aged 65 and older who are receiving Medicare benefits will sustain a hip fracture by the age of 90 [3]. Data from a government study of fracture-related Medicare costs found that in 1991 alone $2.9 billion was spent by Medicare for direct medical costs related to hip fractures [4]. As our population ages, it can only be expected that the cost and impact of fragility fractures to our society will continue to rise.

While there has been progress on the development of new therapies and products to treat and accelerate fracture healing [5], the assessment of fracture healing remains a

subjective process. Clinicians often rely on a combination of the patient's history and clinical findings such as pain, tenderness to palpation, and motion at the fracture site over time to assess progression of healing and thereby make decisions on weight-bearing status and activity level [6]. The problem of monitoring fracture healing is further compounded by the difficulty in developing a consistent definition that is both biologically accurate and clinically relevant. Biological markers such as callus formation, cortical bridging, trabecular patterning, and loss of fracture line, which are easily seen on plain radiograph and commonly used to monitor fracture healing and predict nonunion, have unfortunately shown poor correlation with mechanical strength in laboratory testing [1]. Echo tracking, which noninvasively measures the bending angle around a fracture site under load, has been shown to accurately predict non-union over time [7]; however, this method is operator-dependent and assumes that bone stiffness is directly related to bone strength, which does not necessarily hold true for bone in the remodeling stage of healing [7].

Several studies have used micro-computed tomography (μCT) to measure bone characteristics such as volume and mineral density in a fracture callus [8–11]. A recent study of murine fracture calluses showed a statistically significant correlation between measures of mineralized tissue in fracture calluses (tissue mineral density, mineralized callus volume, standard deviation of mineral density, and bone mineral content) and torsional strength and rigidity as determined by direct mechanical testing [12]. These results suggest that torsional bone strength is directly related to both the geometric and material properties of the fracture callus. Thus, any method for monitoring bone strength during fracture healing must be able to account for both the material properties of bone tissue and the changes in geometry affected by the healing process.

We have previously introduced CT-based rigidity analysis (CTRA) to noninvasively assess the axial, bending, and torsional rigidities of bones from their transaxial cross-sectional images [13] and to predict fracture risk in patients with pathological bone lesions [14, 15]. Rigidity, the product of bone tissue modulus of elasticity and cross-sectional geometry, describes the structural behavior of a bone and its resistance to deformation when subjected to axial, bending, or torsional loads [13, 15, 16]. Modulus of elasticity is a function of bone density, and bone geometry is represented by its cross-sectional area and moment of inertia [17, 18], which quantifies how bone tissue is distributed in space and varies as the fourth power of the distance of the bone tissue relative to a specific bending axis. The CTRA method calculates rigidity by treating bones as simple beams and applying engineering composite beam theory principles, to sum the modulus-weighted area of each pixel comprising the bone section by its position relative to the centroid of the bone in order to assess fracture risk. This method was particularly accurate (97%) at predicting pathological fracture in children with benign bone lesions compared to standard radiographic criteria (42–61% accuracy) [15]. In a study of breast cancer patients with vertebral metastases, the load-bearing capacity calculated from quantitative CT (QCT) data and adjusted for BMI was 70% specific for pathological fractures compared to 20% specificity with standard criteria [14]. Given these promising results in predicting fracture risk, we hypothesize that structural rigidity analysis of bones calculated from μCT data can be used to accurately and quantitatively monitor the progression of fracture healing over time in a rat model of fracture healing. To that end, our aim was to validate the use of structural rigidity analysis in comparison to actual mechanical testing to quantify fracture healing in a rat model of segmental critical defects undergoing human BMP-2 cDNA treatment postsurgery.

Materials and Methods

Overview of Study Design

Critical-sized (5 mm) midfemoral defects were created in the right femurs of 10 adult male Sprague–Dawley rats which were subjected to surgical stabilization by an external fixator. All animals received the human BMP-2 cDNA (4×10^8 plaque-forming units [pfu]) in an adenoviral vector (AdBMP-2) at four time points: two animals received AdBMP-2 intraoperatively (group 1); two animals received AdBMP-2 1 day postsurgery (group 2); three animals received AdBMP-2 5 days postsurgery (group 3); and the last three animals received AdBMP-2 10 days postsurgery (group 4) (Fig. 1).

All animals were killed 8 weeks after surgery, the femora were harvested, and healing was evaluated with μCT-based CTRA and torsional mechanical testing. In the original study [19], delayed administration of the vector resulted in progressive improvement in union and osseous filling and increased torsional strength. Therefore, in order to represent a meaningful range of fracture healing cases, we chose specimens for this study that were subjected to vector administration over a course of 0, 1, 5, and 10 days postsurgery.

Surgical Procedure

An established, critical-sized femoral defect rat model [20] was used in this study. All operative procedures were approved by the Institutional Animal Care and Use Committee. Adult, male Sprague–Dawley rats weighing 400–425 g were placed under general anesthesia by the administration of isoflurane with a small-animal vaporizer.

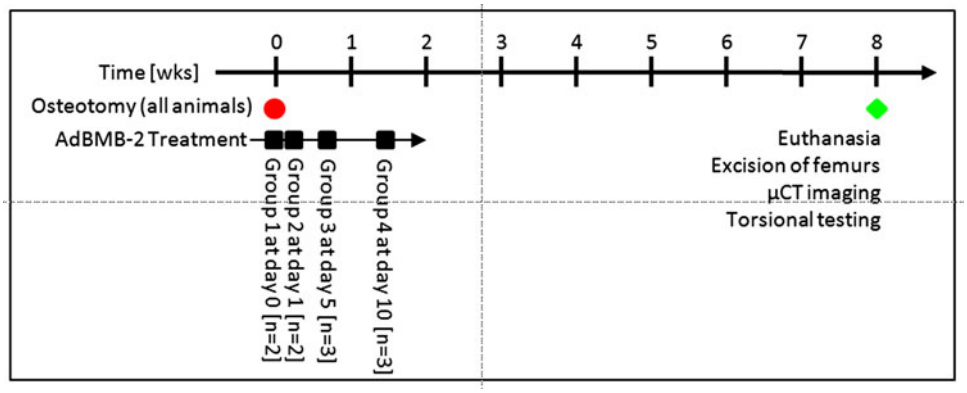

Fig. 1 A timeline of the study

The animals then received intramuscular injections of 20 mg/kg of cefazolin (antibiotic) and 0.08 mg/kg of buprenorphine (analgesic) into the left thigh. The right hindlimb of each animal was shaved and disinfected with povidone iodine. Subsequently, the animals were placed in a sterile field and covered with a surgical drape so that only the prepared limb was exposed. An incision was made in the posterolateral aspect of the right thigh. The lateral intermuscular septum with respect to the femur was dissected to expose the diaphysis of the femur. The periosteum was removed from the anterolateral aspect of the femur, and a fixator template was placed and fastened to the femur with two sterile cable ties. Care was taken to affix the template to allow the pins to be placed in the central portion of the femoral shaft, reducing the likelihood of fracture due to pin placement. Once the template was securely placed, the proximal hole was drilled using a drill guide and a sterile 0.9-mm drill bit. The pin (a 1.1-mm threaded Kirschner wire) was then secured in the femur. The distal pin was placed in the same fashion, with special care taken to place it, and all subsequent pins were placed parallel to the proximal pin. The remaining two pins were placed in the same fashion. The template was then removed, and the skin was pulled over the pins. Small incisions were made to allow the pins to penetrate the skin. The fixator was then secured as close to the skin as possible without risking skin ulcerations.

A 5-mm osteotomy was then performed using a sterile, round dental burr attached to a dental handpiece (AUE-10C/SS Power-Tip; Aseptico, Woodinville, WA). After completion of the osteotomy, the site was copiously irrigated with cefazolin solution. The fascia was closed with 3–0 gut, creating a tight muscle chamber around the defect. The skin incision was closed with 4-0 silk and then cleaned with povidone iodine. The animals were given a 0.10 mg/kg intramuscular injection of buprenorphine for additional analgesia. During the subsequent 2 days, each animal received a 20 mg/kg intramuscular injection of cefazolin once per day and a 0.10 mg/kg intramuscular injection of buprenorphine once every 12 h.

The virus was administered with the rat under general anesthesia and in accordance with National Institutes of Health Biosafety Level-2 (NIH BL-2) guidelines 24 h after surgery. Forty microliters of viral suspension (4×10^8 pfu), appropriately diluted in phosphate-buffered solution, was drawn into an airtight 50-μl Hamilton syringe and administered with a single injection. To ensure accurate injection, a 2-inch (5.1-cm), 22-gauge needle was attached to the barrel of the syringe and inserted into a channel engineered in the external fixator so that the tip of the needle entered the exact center of the defect. The rats were housed in accordance with NIH BL-2 guidelines for 24 h after gene transfer and killed 56 days after treatment. Both femora from each animal were harvested and immediately frozen for μCT and biomechanical testing.

μCT

The segmental defect plus the adjacent bone in the affected limb along with the homologous regions in the contralateral unaffected limb were scanned via μCT imaging (μCT40; Scanco Medical, Brüttisellen, Switzerland) equipped with a 10-mm focal-spot microfocus X-ray tube. The entire defect region was scanned at a 34-μ misotropic voxel size, beam voltage of 55 kVp, current of 145 μA, and integration time of 250 ms. Images were reconstructed and filtered (gaussian filtration with $\sigma = 1.0$), and a threshold was determined using a previously described technique [21]. In order to accurately compare each defective femur with its unaffected counterpart, the orientation of the defective femur was reversed so that it would match the contralateral unaffected limb.

Structural Rigidity Analysis

Rigidity, the product of the bone tissue modulus of elasticity and bone cross-sectional geometry, describes the structural behavior of a bone and its resistance to deformation when subjected to axial loads, bending, or twisting moments. The bone tissue modulus (E) and shear modulus

(G) depend on the bone mineral density. Axial compressive and torsional relationships describing the mentioned mechanical properties of rat bone as a function of μCT-generated density were used to convert the densities to their respective axial and shear modulus values [22, 23]. The bone geometry is represented by the cross-sectional area and moment of inertia (defined as $I_x = \int y^2\, dA$, where y is the distance from the x axis to an infinitesimal area dA). The moment of inertia quantifies how the bone tissue is distributed in space; it varies as the fourth power of the distance of the bone tissue relative to a specific bending axis. The torsional (GJ) rigidity for each transaxial cross section through the bone was calculated by summing the density-weighted area (multiplication of each infinitesimal area [pixel in this case] by its density) of each pixel by its position relative to the density-weighted centroid [16] (Fig. 2). Average GJ (GJ_{AVG}) and minimum GJ (GJ_{MIN}) were reported for each specimen. GJ_{AVG} represents the average torsional rigidity of the entire segment, whereas, GJ_{MIN} represents the torsional rigidity of the entire segment at its weakest cross section. As a bone is as strong as its weakest section [13, 15, 24] and not its average strength, GJ_{MIN} should provide meaningful information on the fidelity of the healed fracture. Sequential transaxial μCT slices were used to generate the average and minimum torsional rigidities of the segmental defects for all specimens and their corresponding contralateral specimens.

Mechanical Testing

Following μCT imaging, all specimens underwent torsional testing to failure using a previously described pure torsion testing system [25]. Both ends of the specimens were embedded in polymethylmethacrylate (PMMA) to provide a uniform interface with the testing module. Specimens were tested to failure under angular displacement control at a constant deformation rate of 5 rad · min^{-1}. Angular deformation and applied load were acquired at a rate of 10 Hz. Torsional stiffness was calculated from the linear region of the slope of the angular displacement-load curve. The torque and rotation data were then used to calculate the torsional stiffness and strength of the healing defect. Shear modulus of elasticity (G), using mechanical testing data, was calculated using a method developed by the authors to assess intrinsic torsional properties of nonhomogenous and non-axisymmetric materials such as a rat femur [23]. Polar moment of inertia (J) was calculated using software developed by Scanco Medical.

Statistical Analysis

In order to determine whether structural rigidity as assessed from μCT imaging can accurately predict failure of bone following creation of structural defects and initiation of fracture healing, specimens were grouped according to testing mode (mechanical vs. CTRA) and a linear regression model was applied. Both average and minimum torsional rigidities as defined by μCT data were analyzed separately against data obtained via mechanical testing. Specimens with and without defects were analyzed together since the validity of structural rigidity analysis should depend only upon the cross-sectional geometry and density of the specimen and not the presence or absence of a defect. The slopes for the two regression models were compared using generalized estimating equations (GEEs)

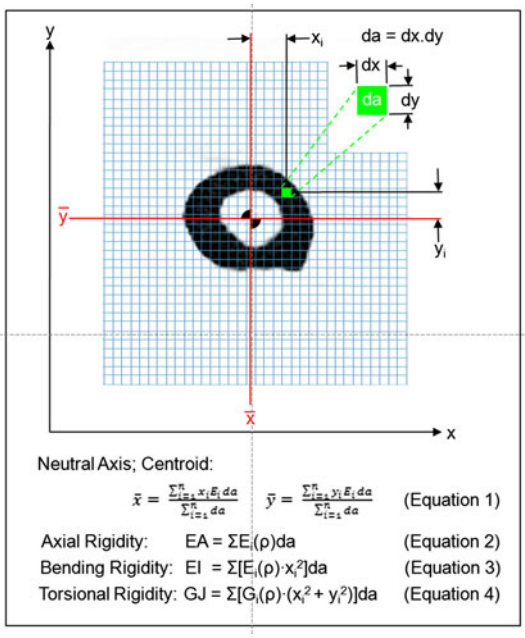

Fig. 2 Schematic diagram illustrating the pixel-based CTRA technique to assess axial (EA), bending (EI), and torsional (GJ) rigidities. Each grid element is intended to represent one pixel (the exaggeration of the grid element size is solely for illustration purposes). The EA, EI, and GJ equations are presented here, where ρ represents bone density; x_i and y_i represent the distance of each pixel from the y and x axes, respectively; da represents the area of each pixel; E_i represents Young's modulus of elasticity (defined as the ratio of tensile strength to strain in the linear region); and G_i represents shear modulus (defined as the ratio of shear stress to shear strain in the linear region). Each pixel is filtered through a bone density threshold and converted to material modulus (E or G depending on the loading mode) and using empirically derived relationships for rat bone as a function of bone density. The relative distance between pixels is determined by the calibration of the imaging modality. The modulus-weighted neutral axis and centroid (Eq. 1) are determined based on the coordinates of pixel i, its modulus (E_i), area (da), and total number of pixels in the bone cross section (n). Axial rigidity (Eq. 2) is the sum of the products of each pixel's elastic modulus (E_i) and pixel area (da). Bending rigidity about the y-axis (Eq. 3) is the sum of the products of the elastic modulus (E_i), square of pixel i distance to the neutral axis (y), and the pixel area (da). Torsional rigidity (Eq. 4) is the sum of the products of the density-dependent shear modulus (G_i), the square of the pixel distance to the centroid $(\bar{x}, \bar{y})$, and the pixel area (da)

with the appropriate Wald test for comparing slopes between groups. Differences in the magnitude of R^2 values were compared using analysis of covariance.

Paired Student's *t*-test was used to assess whether GJ values obtained from mechanical testing vs. CTRA-based average and minimum GJ values were significantly different from one another.

Statistical analysis was performed using the SPSS software package (version 16.0; SPSS, Inc., Chicago, IL). Two-tailed values of $P < 0.05$ were considered statistically significant.

Results

CTRA-based GJ_{AVG} was moderately correlated with torsional rigidity assessed from mechanical testing results ($R^2 = 0.63$, Fig. 3). This correlation improved significantly when the CTRA-based GJ_{MIN} was correlated to the mechanical testing-based results ($R^2 = 0.81$, Fig. 4). The slopes of the two regression models were not different from one another ($P = 0.67$), yet the *y*-intercept values of the two regression models were different ($P < 0.001$). No significant differences were observed between the CTRA-based GJ_{MIN} and those obtained from mechanical testing based on paired *t*-test analysis ($P = 0.43$). However, the CTRA-based GJ_{AVG} was statistically different from the GJ data obtained from mechanical testing results when subjected to paired analysis ($P < 0.001$). CTRA-based GJ_{MIN} was also well-correlated to strength ($R^2 = 0.78$).

Based on mechanical testing results, femurs with defect undergoing AdBMP-2 treatment at different time points

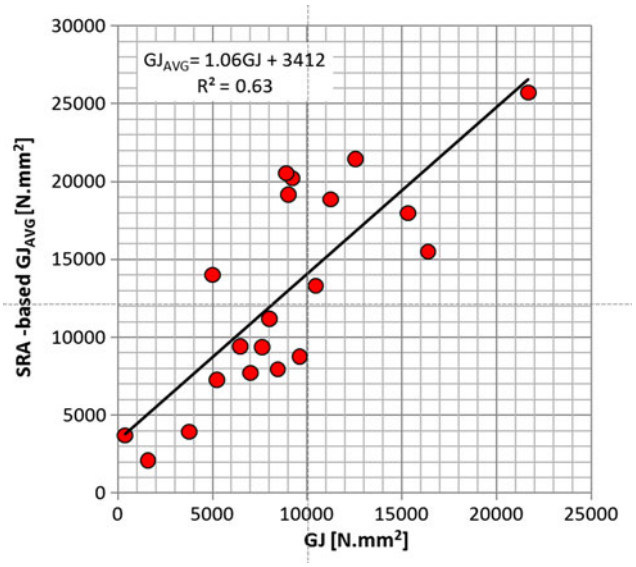

Fig. 3 Average mechanical testing-based versus CTRA-based GJ correlations

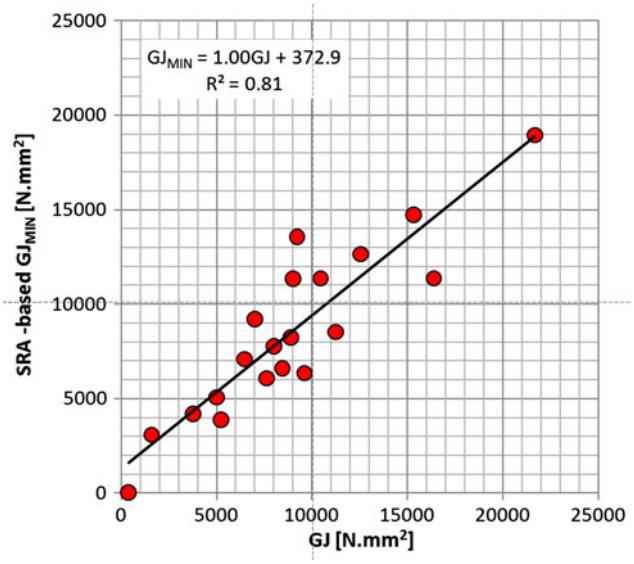

Fig. 4 Minimum mechanical testing-based versus CTRA-based GJ correlations

regained 5–166% of their torsional strength when compared to their respective contralateral specimens. The CTRA-based GJ_{MIN} placed this ratio at 2–163%, whereas the CTRA-based GJ_{AVG} resulted in a range of 15–218%. The defect femurs that had regained a smaller portion of their torsional strength, in comparison to their contralateral specimens, belonged to the early AdBMP-2 administration groups (0 and 1 day postoperation), whereas the bones that regained most of their torsional strength, and in some cases exceeded the torsional strength of the contralateral specimens, belonged to the delayed AdBMP-2 administration groups (5 and 10 days postoperation).

Further coefficients of determination are shown in Table 1, where bone mineral density (BMD, $g \cdot cm^{-2}$) and bone mineral content (BMC, g), obtained from dual-energy X-ray absorptiometry, were correlated with GJ ($R^2 = 0.51$ and 0.48) and peak torque ($R^2 = 0.32$ and 0.30) assessed from mechanical testing.Polar moment of inertia (J) was also correlated with peak torque ($R^2 = 0.46$). These coefficients of determination are significantly different from

Table 1 Correlations between GJ and peak torque values obtained from mechanical testing and BMD, BMC, SSI, and polar moment of inertia

	GJ	Peak torque
CTRA-based GJ_{MIN}	$R^2 = 0.81$	$R^2 = 0.78$
CTRA-based GJ_{AVG}	$R^2 = 0.63$	–
SSI	$R^2 = 0.70$	–
BMD	$R^2 = 0.51$	$R^2 = 0.32$
BMC	$R^2 = 0.48$	$R^2 = 0.30$
Moment of inertia	N/A	$R^2 = 0.46$

those reported previously between CTRA-based GJ values and mechanical testing-based GJ ($P \leq 0.05$ for all cases).

Discussion

Despite continued development of new therapies and treatments to accelerate fracture healing, accurate, noninvasive measurement of the healing process remains an elusive task. The results of this study support the hypothesis that progression of fracture healing over time can be accurately and quantitatively monitored in a rat model by conducting structural rigidity analysis on serial axial μCT images of the affected bone. Torsional rigidity measured noninvasively by μCT was well-correlated with the results of mechanical testing. Minimum torsional rigidity produced a stronger correlation with mechanical testing results ($R^2 = 0.81$) (Fig. 4) than average torsional rigidity ($R^2 = 0.63$) (Fig. 3). These coefficients of determination were superior and significant in comparison to those obtained between mechanical testing-based torsional rigidity and peak torque vs. BMD, BMC, and polar moment of inertia. Furthermore, paired Student's *t*-test showed no significant difference in torsional rigidity as determined by CTRA using minimum GJ and mechanical testing ($P = 0.43$). However, this was not the case for CTRA using average GJ when compared to mechanical testing data reaching statistical significance ($P < 0.0001$). This is partially due to the inherent reduction of noise with minimum torsional rigidity measurements; however, this also suggests that minimum torsional rigidity is a better model for predicting bone failure than average torsional rigidity. This corresponds to expected behavior, where the weakest point, and not the average strength, determines the failure of a beam under angular displacement.

In the average and minimum torsional rigidity models, the slope of the linear regressions was 1.0, indicating that CTRA is correlated without any skewness with mechanical testing results over the full range of values tested. The linear regression model for average torsional rigidity produced a large offset ($y_0 = 3{,}412$), suggesting that CTRA using average torsional rigidity consistently overpredicts bone strength. As expected, this was improved by using minimum torsional rigidity ($y_0 = 372.9$). This lends further support to the hypothesis that minimum torsional rigidity is more accurate than average torsional rigidity at predicting the strength of healing bone.

Previous studies have shown that progression of fracture healing over time is strongly linked to an increase in both callus size and tissue mineral density [12, 26–28]. In this study, torsional strength regained after fracture varied from 5% to 166% and depended on the distribution of callus formation relative to the neutral axis. While the sample size in this study was relatively small, larger calluses were consistently seen with later BMP injections, resulting in a larger distribution of bone around and away from the neutral axis. This increased the torsional strength of the affected bone but resulted in poorly organized bone. Time of BMP injection had no effect on the correlation between torsional rigidity as determined by CTRA vs. mechanical testing.

The results of this study corroborate the recent findings of Morgan et al. [12] that μCT-derived metrics can accurately predict the mechanical properties of fracture calluses. In a principal component analysis of 188 murine fracture calluses under a range of experimental conditions predicted to effect fracture healing, Morgan et al. [12] demonstrated that both quantity and mineral density of newly formed bone were highly correlated with torsional rigidity. A recent study by Nyman et al. [11] also demonstrated a correlation between callus mineral density and callus strength in rat femora. Their data also suggest a relationship between callus geometry through degree of closure of the fracture gap and callus strength [11]. Kokoroghiannis et al. [29] correlated strength-strain index (SSI) as derived from peripheral QCT (pQCT) data in rabbit tibias undergoing distraction osteogenesis to bone stiffness ($R^2 = 0.716$) and proposed pQCT as a method for predicting bone failure following frame removal based on this correlation. SSI described 70% of the variation in mechanical testing-based GJ, which was different from CTRA-based GJ_{AVG} ($R^2 = 0.63$, superior) and GJ_{MIN} ($R^2 = 0.81$, inferior) ($P < 0.05$ for both cases). This study proposes that not only is there a correlation between μCT-derived data and bone strength but structural rigidity analysis based on μCT data can be successfully employed to noninvasively assess the progression of fracture healing. This technique is independent of both type of bone and state of bone repair. The advantage of this technique is its usage of structural engineering principles to calculate load capacity of bone rather than relying on purely correlative data.

In summary, the results of this study suggest that structural rigidity analysis of μCT data can be used to accurately and quantitatively measure the progression of fracture healing over time in an experimental rat model. As expected by an analysis of the biophysics of bone subjected to mechanical load, minimum torsional rigidity proved a better model for measuring bone strength than average torsional rigidity. It remains to be seen whether analogous CT images in human patients could also be used to monitor fracture healing and predict non-union. Future study across multiple fracture modalities and imaging techniques involving larger sample sizes is warranted to evaluate the reproducibility and extensibility of these promising results. However, the results of this study suggest considerable potential in the use of μCT-based CTRA to quantitatively and noninvasively assess fracture healing.

Acknowledgements The authors acknowledge the National Institutes of Health (R01 award AR050243, to C. H. E.) for funding a portion of this study. Additionally, the authors acknowledge the insightful comments made by the reviewer.

References

1. Morshed S, Corrales L, Genant H, Miclau T 3rd (2008) Outcome assessment in clinical trials of fracture-healing. J Bone Joint Surg Am 90(Suppl 1):62–67
2. Finkelstein EA, Corso PS, Miller TR (2006) The incidence and economic burden of injuries in the United States. Oxford University Press, New York
3. Barrett JA, Baron JA, Karagas MR, Beach ML (1999) Fracture risk in the U.S. Medicare population. J Clin Epidemiol 52:243–249
4. Centers for Disease Control, Prevention (1996) Incidence and costs to Medicare of fractures among Medicare beneficiaries aged ≥65 years—United States, July 1991–June 1992. MMWR Morb Mortal Wkly Rep 45:877–883
5. Betz OB, Betz VM, Nazarian A, Pilapil CG, Vrahas MS, Bouxsein ML, Gerstenfeld LC, Einhorn TA, Evans CH (2006) Direct percutaneous gene delivery to enhance healing of segmental bone defects. J Bone Joint Surg Am 88:355–365
6. Firoozabadi R, Morshed S, Engelke K, Prevrhal S, Fierlinger A, Miclau T III, Genant HK (2008) Qualitative and quantitative assessment of bone fragility and fracture healing using conventional radiography and advanced imaging technologies—focus on wrist fracture. J Orthop Trauma 22:S83–S90
7. Matsuyama J, Ohnishi I, Sakai R, Bessho M, Matsumoto T, Miyasaka K, Harada A, Ohashi S, Nakamura K (2008) A new method for evaluation of fracture healing by echo tracking. Ultrasound Med Biol 34:775–783
8. Duvall CL, Taylor WR, Weiss D, Wojtowicz AM, Guldberg RE (2007) Impaired angiogenesis, early callus formation, and late stage remodeling in fracture healing of osteopontin-deficient mice. J Bone Miner Res 22:286–297
9. Schmidhammer R, Zandieh S, Mittermayr R, Pelinka LE, Leixnering M, Hopf R, Kroepfl A, Redl H (2006) Assessment of bone union/nonunion in an experimental model using microcomputed technology. J Trauma 61:199–205
10. Shefelbine SJ, Simon U, Claes L, Gold A, Gabet Y, Bab I, Muller R, Augat P (2005) Prediction of fracture callus mechanical properties using micro-CT images and voxel-based finite element analysis. Bone 36:480–488
11. Nyman JS, Munoz S, Jadhav S, Mansour A, Yoshii T, Mundy GR, Gutierrez GE (2009) Quantitative measures of femoral fracture repair in rats derived by micro-computed tomography. J Biomech 42:891–897
12. Morgan EF, Mason ZD, Chien KB, Pfeiffer AJ, Barnes GL, Einhorn TA, Gerstenfeld LC (2009) Micro-computed tomography assessment of fracture healing: relationships among callus structure, composition, and mechanical function. Bone 44:335–344
13. Hong J, Cabe GD, Tedrow JR, Hipp JA, Snyder BD (2004) Failure of trabecular bone with simulated lytic defects can be predicted non-invasively by structural analysis. J Orthop Res 22:479–486
14. Snyder BD, Cordio MA, Nazarian A, Kwak SD, Chang DJ, Entezari V, Zurakowski D, Parker LM (2009) Noninvasive prediction of fracture risk in patients with metastatic cancer to the spine. Clin Cancer Res 15(24):7676–7683
15. Snyder BD, Hauser-Kara DA, Hipp JA, Zurakowski D, Hecht AC, Gebhardt MC (2006) Predicting fracture through benign skeletal lesions with quantitative computed tomography. J Bone Joint Surg Am 88:55–70
16. Lai W, Rubin D (1993) Introduction to continuum mechanics. Butterworth-Heinemann, Boston
17. Martin RB (1991) Determinants of the mechanical properties of bones. J Biomech 24(Suppl 1):79–88
18. Turner CH (2002) Determinants of skeletal fragility and bone quality. J Musculoskelet Neuronal Interact 2:527–528
19. Betz OB, Betz VM, Nazarian A, Egermann M, Gerstenfeld LC, Einhorn TA, Vrahas MS, Bouxsein ML, Evans CH (2007) Delayed administration of adenoviral BMP-2 vector improves the formation of bone in osseous defects. Gene Ther 14:1039–1044
20. Einhorn TA, Lane JM, Burstein AH, Kopman CR, Vigorita VJ (1984) The healing of segmental bone defects induced by demineralized bone matrix. A radiographic and biomechanical study. J Bone Joint Surg Am 66:274–279
21. Alexander J, Bab I, Fish S, Müller R, Uchiyama T, Gronowicz G, Nahounou N, Zhao Q, White D, Chorev M, Gazit D, Rosenblatt M (2001) Human parathyroid hormone 1–34 reverses bone loss in ovariectomized mice. J Bone Min Res 16:1665–1673
22. Cory E, Nazarian A, Entezari V, Vartanians V, Müller R, Snyder BD (2010) Compressive axial mechanical properties of rat bone as functions of bone volume fraction, apparent density and micro-CT based mineral density. J Biomech 43(5):953–960
23. Nazarian A, Entezari V, Vartanians V, Müller R, Snyder BD (2009) An improved method to assess torsional properties of rodent long bones. J Biomech 42(11):1720–1725
24. Whealan KM, Kwak SD, Tedrow JR, Inoue K, Snyder BD (2000) Noninvasive imaging predicts failure load of the spine with simulated osteolytic defects. J Bone Joint Surg Am 82:1240–1251
25. Nazarian A, Bauernschmitt M, Eberle C, Meier D, Muller R, Snyder BD (2008) Design and validation of a testing system to assess torsional cancellous bone failure in conjunction with time-lapsed micro-computed tomographic imaging. J Biomech 41: 3496–3501
26. Augat P, Merk J, Genant HK, Claes L (1997) Quantitative assessment of experimental fracture repair by peripheral computed tomography. Calcif Tissue Int 60:194–199
27. den Boer FC, Bramer JA, Patka P, Bakker FC, Barentsen RH, Feilzer AJ, de Lange ES, Haarman HJ (1998) Quantification of fracture healing with three-dimensional computed tomography. Arch Orthop Trauma Surg 117:345–350
28. Jamsa T, Koivukangas A, Kippo K, Hannuniemi R, Jalovaara P, Tuukkanen J (2000) Comparison of radiographic and pQCT analyses of healing rat tibial fractures. Calcif Tissue Int 66:288–291
29. Kokoroghiannis C, Charopoulos I, Lyritis G, Raptou P, Karachalios T, Papaioannou N (2009) Correlation of pQCT bone strength index with mechanical testing in distraction osteogenesis. Bone 45:512–516